Semi-continuous temperature cycle-induced deracemization using an axially chiral naphthamide

Ryusei Oketani[*†a], Riku Naito[†a], Ichiro Hisaki[*a]

[a]Division of Chemistry, Graduate School of Engineering Science, Osaka University, 1-3 Machikaneyama, Toyonaka, Osaka 560-8531, Japan.

[†]These authors are equally contributed to the work. All authors agreed to switch the order of the first and second authors in their personal CV.

Abstract

This study outlines a practical semi-continuous method for temperature cycle-induced deracemization (TCID) using a batch mode crystallizer. We employed an axially chiral naphthamide derivative as a model compound, and deracemized the crystalline phase by conventional TCID. To achieve a continuity of deracemization, we harvested a part of the suspension after the conventional TCID, then feeding a new racemic suspension into the enriched suspension and applying temperature cycles. By leaving a highly enriched crystalline phase as seed crystals to direct the chirality of the following enrichment, the enrichment process was significantly accelerated, verifying the stable and high production efficiency. Furthermore, from the perspective of process productivity, the moderate suspension density is optimal for efficient deracemization. In the naphthamide system, up to 7.71 $g \cdot L^{-1} \cdot h^{-1}$ of the productivity was achieved. Thanks to the simple operation, the method described here is applicable for most of batch mode deracemization reported to date. In terms of industrial application, the semi-continuous deracemization could be a good option to utilize the existing batch crystallizers.

Keywords: deracemization, continuous crystallization, chiral separation, process engineering

Introduction

Continuous production is projected to be adopted in the pharmaceutical industry, and the field of continuous synthesis of compounds has shown significant progress.[1–4] The continuous purification process represents a critical foundational technology for establishing fully continuous production. Resolution of chiral compounds are essential techniques for efficient separation and purification,[5] and resolution by crystallization, a method applicable to compounds forming conglomerate, is a vital development subject due to its simplicity and scalability.[6–8] The preferential crystallization has been widely used as a classic resolution,[9–15] and its continuous operation has been thoroughly studied through various methods such as the mixed suspension mixed product removal (MSMPR) method,[16,17] coupled preferential crystallization,[17–20] and fluidized bed crystallization.[21–23] However, when the products are racemate, the theoretical maximum yield of preferential crystallization is 50%.[24,25]

In contrast, deracemization by crystallization, a crystallization process of a conglomerate under racemization conditions, reaches 100% of maximum yield, because the undesired enantiomer is converted into the desired one while being removed from equilibrium in solution phase. Following Viedma's report,[26] comprehensive studies have been reported on its application to various compounds[27–37] and model simulations[38–44] to understand mechanism behind the process. However, most of the deracemization processes developed so far involve batch mode operations, and industrial application to processes has not been successful. In fact, simple scale-up for a batch mode operation is limited by the solubility of the target compound and the size of the crystallizer.

Pioneering examples of continuous deracemization by flow mode continuous crystallization have been reported by Cameli and coworkers.[45] They demonstrated for the first time that complete continuous and automated deracemization of crucial chiral drug intermediates is enabled by utilizing spatial thermal vibrations within a tubular flowing millireactor. Moreover, the potential to apply continuous crystallization processes to deracemization has been sufficiently verified in modeling studies.[38,40,46] On the other hand, a batch mode crystallizer is easy to introduce for high-mix, low-volume production because it can use existing systems and is a facile operation. However, continuous systems for deracemization using batch mode crystallizer have not been experimentally validated since most deracemizations require considerable time for enrichment. Therefore, a very long residence time is necessary, and its control is difficult.

In this study, we demonstrate a straightforward semi-continuous process for temperature cycle-induced deracemization using a batch mode crystallizer. By enriching via TCID and subsequent crystal removal and addition of a racemate, we accomplished semi-continuous deracemization with simple operations. The key to this method is leaving part of the enriched crystal as seed crystals to control the chirality of the following enrichment process, enabling the progression of deracemization from a relatively high enriched state. The semi-continuous process ensures sufficiently long residence time which allows the time for completing deracemization. Furthermore, we observed the size of crystals during deracemization, and the mechanism how the feed crystals are incorporated to the crystals. These observations would contribute to monitor the progress of deracemization without off-line analysis.

Materials and methods

We used the axially chiral compound **1** as a model compound (Scheme 1). This compound was first reported by Sakamoto and coworkers,[47] and we previously reported the modified synthetic procedure for 100-g scale synthesis.[28] This compound forms a stable conglomerate by crystallizing from conventionally used solvents except for methanol and exhibits spontaneous racemization behavior in the solution due to the rotation of the C−C bond. However, the activation energy of rotation in methanol is enough high to evaluate enantiomeric excess by HPLC.[28] Technical grade ethyl acetate, cyclohexane, and *tert*-butylmethyl ether (MTBE) are purchased from Nacalai Tesque, and used without further purification.

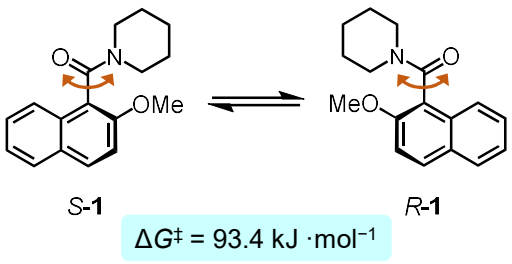

Scheme 1. Chemical structure of axially chiral naphthamide derivative **1**. The value of Gibbs free energy of activation ($\Delta G^{\ddagger}$) is measured in methanol. The half-life time at 20 °C is 367 min.

Solubility measurements

The solubility of **1** in MTBE and in an azeotropic mixture of cyclohexane and ethyl acetate was measured in triplicate by using a gravimetric method. The temperature was controlled by a thermostat (NCB-1210, EYELA, Japan).

Chiral HPLC analysis

The accurate chiral composition of **1** in solid samples was analyzed by a HPLC system (PU-980, UV980, JASCO) using an CHIRALPAK IA-3 (Daicel, 3 μm, 150 mm × 4.6 mm) and a mixture of hexane and ethanol (7:3, v/v) as the mobile phase at a flow rate of 1.5 mL·min^{-1}. The wavelength employed for UV detection was 254 nm. Note that while compound **1** spontaneously racemizes in solution, the racemization is sufficiently slow in cold methanol, allowing the analysis to be performed while maintaining the *ee* of the crystalline phase. To suppress racemization during analysis, the column temperature was controlled at 0 °C using a portable refrigerator. The enantiomeric excess (*ee*) values were obtained by integrating and comparing the peak areas of *R*-**1** and *S*-**1** according to the following equation (eq.1).

$$\textit{enantiomeric excess}\ (\%) = \frac{A_R - A_S}{A_R + A_S} \qquad \text{(eq.1)}$$

where A_R and A_s is the area in HPLC analysis for *R*-**1** and *S*-**1** respectively.

Batch-type TCID

30 mL of screw vial was charged with compound **1** and MTBE or ethyl acetate/cyclohexane azeotropic mixture (10 mL), and was heated until the solid was completely dissolved. The solution was immersed in an ice bath, and rapid crystallization was carried out by irradiating with ultrasound for preparing a racemic suspension. A beaker equipped with a double glass jacket was filled with water, and a coolant was circulated inside the glass jacket. The temperature of the coolant was controlled by a cooling circulator (NCB-1210, EYELA, Japan). The cooling circulator was connected to a computer *via* an RS232C cable, and the temperature was controlled through software (EPMon, EYELA, JAPAN). The temperature cycles were performed between 15 °C and 30 °C, and were set to last 40 minutes per cycle. During the temperature cycle, the suspension was constantly stirred

by a crossbar-type Teflon stirrer bar at a rotation speed of 300 rpm. The *ee* of the crystalline phase was determined every few cycles by chiral HPLC analysis on a small amount of solid taken from suspension.

Semi-continuous TCID

TCID in a semi-continuous manner was performed using the set-up shown in Figure 1a, and the operation procedure was briefly described in Figure 1b. Compound **1** was added to a 500 mL flask containing MTBE 300 mL and a cross-shape PTFE stirrer bar. The mixture was heated until the compound was completely dissolved. Then, while cooling the solution with ice, ultrasound was irradiated to rapidly cool it, allowing to prepare a racemic suspension. This was transferred to a 500 mL flask equipped with a double glass jacket, and stirred using a mechanical stirrer (MAZELA Z, EYELA, Japan) at 150 rpm, the temperature of the coolant was controlled by a circulating thermostat (EYELA NCB-1210, EYELA, Japan) as shown in Figure 1a. The set temperature of the coolant and the actual suspension temperature were monitored to ensure whether they matched the desired temperature cycle profile. To monitor the *ee* of the crystalline phase during racemization, a small amount of suspension was collected and dissolved in ice-cold MeOH, and evaluated using the chiral HPLC. When the *ee* reached 90%, suspension was collected by a peristaltic pump (120U/DV, Watson-Marlow, UK) for 6 minutes with the rate of 25 mL min^{-1}. Additional suspension prepared beforehand to match the initial suspension density was poured into the crystallizer. By this procedure, the collected suspension was replaced with an equal volume of racemic suspension. After 5 times collections of the enriched suspension, the semi-continuous process was suspended. The process productivity of the semi-continuous process was evaluated by taking a time after the first addition of suspension because the process can run as long as the racemic suspension is added to the system after initial enrichment.

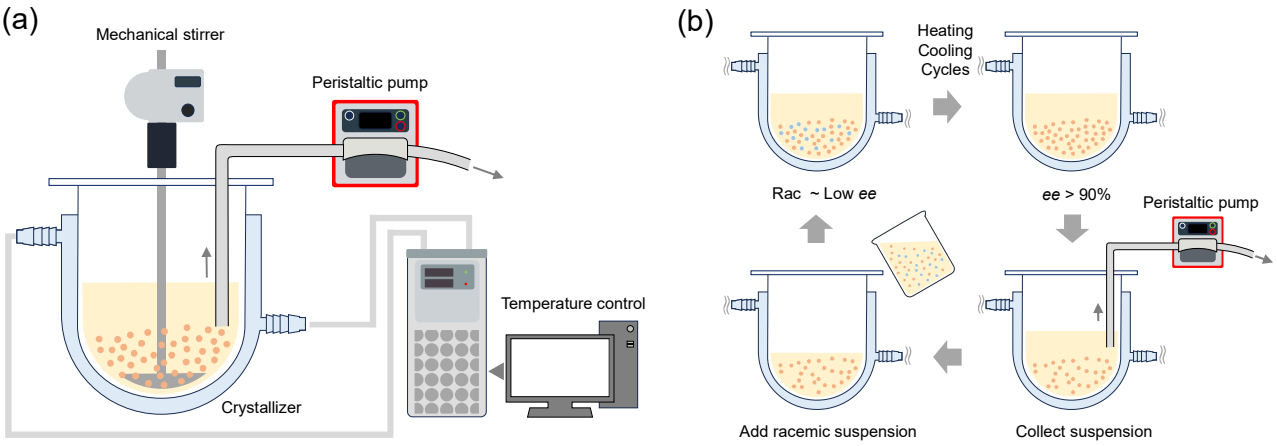

Figure 1. (a) Semi-continuous crystallization setup and (b) procedure of the manipulation. Racemic suspension for feeding and initial suspension are prepared by flash cooling of saturated solution of **1** with sonication.

Results and discussion

Initial enrichment by TCID

The solubilities of **1** in ethyl acetate/cyclohexane azeotropic mixture were 6.09 wt% at 20 °C and 8.93 wt% at

30 °C, and in MTBE were 1.85 wt% at 15 °C and 3.35 %wt at 30 °C (See Supporting Information). For each solvent system, TCID was conducted at a suspension density where 30% to 90% of the crystals interconvert at temperature cycles of 15 °C or 20 °C and 30 °C. Chiral enrichment by TCID was confirmed under all suspension density in both solvent systems (Figure 3). It should be noted that a racemate was used as the starting condition, and no seeding or induction was performed, resulting in random final chirality. Although there is some variation in the onset of chiral enrichment under all conditions, it can be explained as the stochastic behavior due to fluctuations arising in open non-equilibrium systems, as proposed in the dynamic symmetry-breaking model in a non-equilibrium steady state by Kondepudi and Asakura.[48] That is, when the *ee* of the system is close to zero, *ee* fluctuates around zero, then showing enrichment right after it exceeds a critical value. With smaller suspension densities, the amount of interconversion and fluctuation are greater, leading to significant variation in the onset. The enrichment curve for each TCID also exhibits a sigmoidal shape, similar to many TCIDs reported so far.

Focusing on the required period to complete deracemization in MTBE, it was observed that the required period is shorter under conditions of smaller suspension density as shown in Figure 3. However, production efficiency was highest when the suspension density was moderate, indicating that efficiency decreases when the suspension density is either too low or too high as shown in Figure 4a. At low suspension densities, the process completes very quickly, precluding further acceleration. For instance, a condition with a suspension density of 1.8×10^{-2} kg-solid/kg-solvent in MTBE corresponds to 90% of the solid dissolving/crystallizing in a single temperature cycle, which requires at least two cycles even under ideal conversion. The condition with the suspension density of 2.3×10^{-2} kg· kg^{-1} leads to 70% dissolving/crystallizing, also necessitating two cycles. If these conditions complete deracemization in two cycles, the process productivity for the suspension density of 2.3×10^{-2} kg· kg^{-1} is higher than one of 1.8×10^{-2} kg· kg^{-1} because the amount of crystals in the suspension is much. In fact, the number of temperature cycles required for deracemization is five times for 1.8×10^{-2} kg· $kg^{-1}$and two times for 2.3×10^{-2} kg· kg^{-1} (Figure 3), the deracemization completed faster for the condition of 2.3×10^{-2} kg· kg^{-1}, and its process productivity is much higher than the condition of 1.8×10^{-2} kg· kg^{-1}. This fact also suggests a problem of crystal growth under conditions where the suspension density is too low. Namely, there is a shortage of crystals needed for crystal growth, resulting in the primary nucleation of the minor enantiomer, *i.e.*, nucleation occurs with random chirality. Conversely, at a suspension density of 2.3×10^{-2} kg· kg^{-1}, an adequate number of particles remain during crystal growth, leading efficient process progression. These experimental results imply that an optimal balance between suspension density and temperature cycle exists for efficient deracemization.

In the case of deracemization in the mixture of cyclohexane and ethyl acetate, the period required to complete enrichment showed similar trend to the case of MTBE. However, the smallest suspension density (3.7×10^{-2} $kg\cdot kg^{-1}$) gave the highest process productivity, 2.58 g· h^{-1}· L^{-1}. In this solvent, even if the suspension densities are reduced to increase the interconversion in one temperature cycle, deracemization does not proceed ideally, requiring many temperature cycles. As shown in Figure 3h, even 90% of crystals are replaced in one temperature

cycle, more than 15 temperature cycles were required to complete deracemization. Therefore, the smaller the suspension densities result the faster the deracemization in this system, and shorter period required to complete deracemization can lead higher productivity. In such a system, the balance between the amount of crystals that can be handled in a single operation and the time required to complete the enrichment is important for determining efficiency.

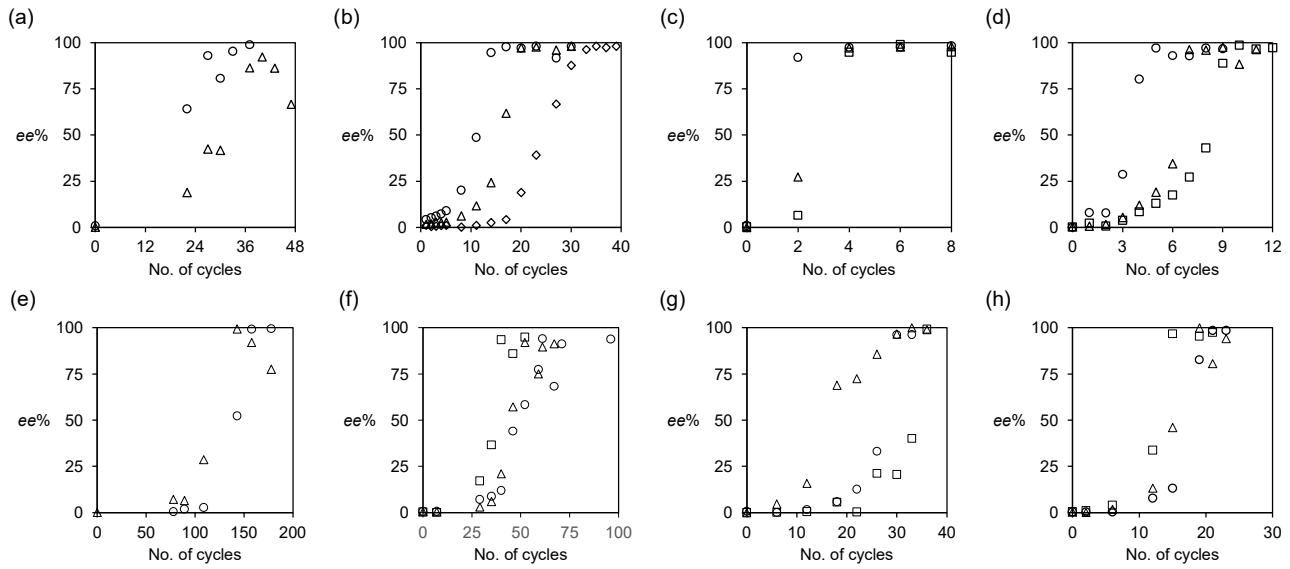

Figure 3. Evolution of enantiomeric excess of **1** during batch-wise TCID for different suspension densities in (a−d)MTBE and (e−h)cHex/EtOAc = 54/46 (v/v). Absolute values of enantiomeric excess (*ee*) are used in the vertical axes. Suspension densities are (a) 5.3×10^{-2} kg·kg^{-1} (b) 3.2×10^{-2} kg·kg^{-1} (c) 2.3×10^{-2} kg·kg^{-1} (d) 1.8×10^{-2} kg·kg^{-1} (e) 11.1×10^{-2} kg·kg^{-1} (f) 6.6×10^{-2} kg·kg^{-1} (g) 4.7×10^{-2} kg·kg^{-1} (h) 3.7×10^{-2} kg·kg^{-1}.

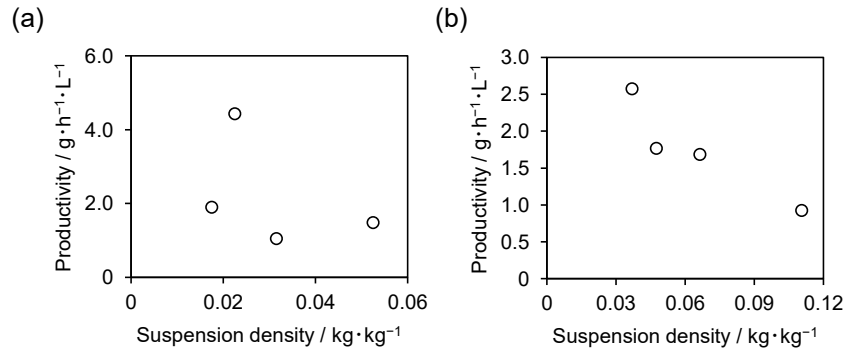

Figure 4. Process productivities for different suspension densities in (a) MTBE and (b) cHex/EtOAc = 54/46 (v/v).

Semicontinuous TCID

Semi-continuous deracemization was conducted using batch mode crystallizers after the initial enrichment carried out in same manner to the conventional TCID. The crystalline phase was periodically sampled to monitor

the *ee*, and once it exceeded 90%, the part of suspension was collected, and racemic suspension was fed to the flask. Figure 5 show the time course of *ee* during semi-continuous mode after initial enrichment. As shown in Figure 5a, the temporal decrease in *ee* after the collection of suspension and the addition of racemic a suspension was observed for the condition of suspension density of 5.3×10^{-2} kg·kg^{-1}. Then, the *ee* of crystals recovered through temperature cycling. This trend was also seen when the suspension density was 3.9×10^{-2} kg·kg^{-1}, but the amount of decrease in *ee* was smaller, and the time needed for recovery was shorter (Figure 5b). This indicates that at smaller suspension densities, deracemization proceeds quickly. Interestingly, this rate of recovery reached maximal under conditions where the suspension density was 3.2×10^{-2} or

less, the *ee* of crystals was fully recovered within 1-2 cycles even after adding the racemic suspension as shown in Figure 5c–e. In other words, under the conditions of these suspension densities, it is possible to continue to remove crystals and add racemic suspensions at every temperature cycle. This behavior is different from the one from a similar *ee* in batch mode TCID, and is expected to benefit from the presence of enriched crystals. In terms of process productivity, the condition with the suspension density of 3.2×10^{-2} kg·kg^{-1} where the rate of recovery reached maximum gave maximum value, 7.71 g·L^{-1}·h^{-1}. This is the 1.7 times greater than batch mode TCID at the same suspension density. Additionally, the direction of enrichment never reversed once enriched, consistently leading to the same chirality.

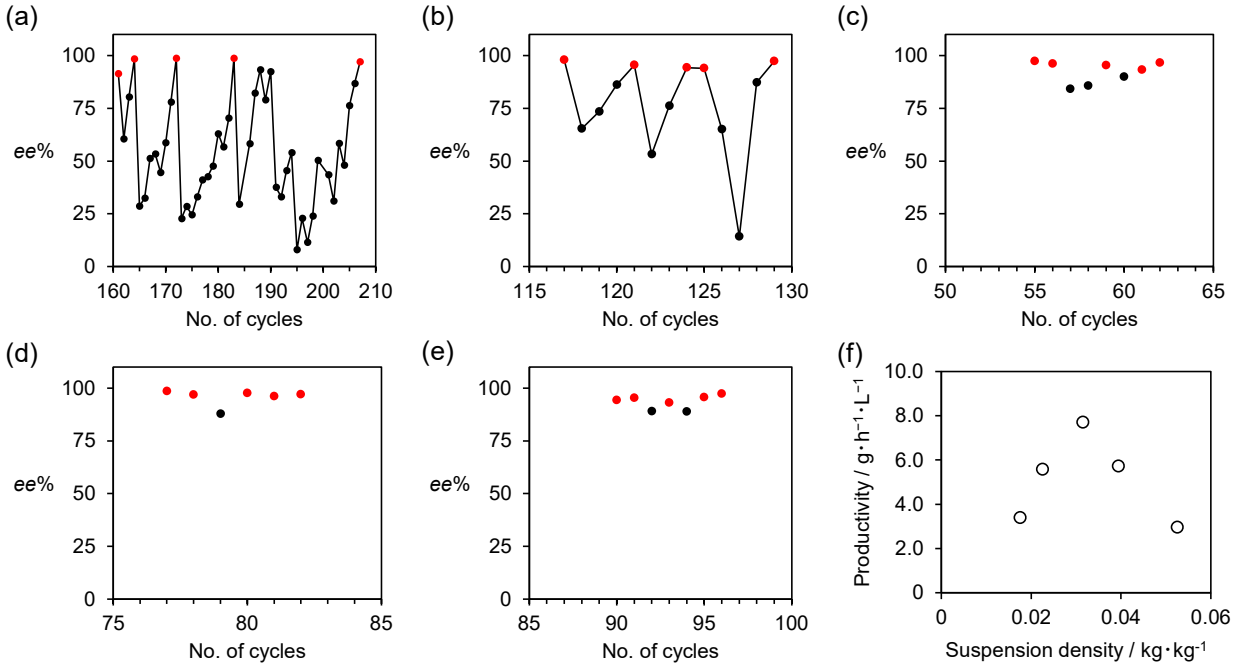

Figure 5. (a–e) Evolution of *ee* of **1** during semi-continuous TCID in MTBE after initial enrichment for different suspension densities, and (f) process productivities. Lines in (a) and (b) are guide for eyes. Suspension densities are (a) 5.3×10^{-2} kg·kg^{-1} (b) 3.9×10^{-2} kg·kg^{-1} (c) 3.2×10^{-2} kg·kg^{-1} (d) 2.3×10^{-2} kg·kg^{-1} (e) 1.8×10^{-2} kg·kg^{-1}.The red symbols indicate when racemic suspensions added.

Changes in crystal size were observed with the progression of semi-continuous deracemization. Figure 6 shows the crystal growth during semi-continuous deracemization in MTBE. At the initial stage of deracemization, rapid nucleation and crystallization caused by ultrasound resulted in the predominance of tiny crystals measuring 5–10 μm. Moreover, the morphology of these crystals was mostly random (Figure 6c, Cycle 0). However, when temperature cycles were applied, the repeated dissolution and crystallization gradually increased the crystal size, leading to more uniform shapes despite some aggregation (Figure 6c, Cycle 47 and 75). The solubility of the crystalline phase is known to vary with particle size due to the Gibbs-Thomson effect, with larger crystals growing by incorporating smaller ones.[49] As the tiny crystals were incorporated, a convergence to a certain shape and crystal size occurred, followed by a gradual increase in *ee* of the crystals. At the point when *ee* exceeded 90%, almost no tiny crystals were observed, and the crystal size converged to around 25–30 μm (Figure 6c, Cycle 161). Subsequently, when a racemic suspension was added, aggregation of tiny crystals around the enriched crystals was observed (Figure 6c, Cycle 162). These aggregated crystals caused decreased *ee*, containing a significant amount of the opposite enantiomer. However, repeating the temperature cycles resulted these tiny crystals to disappear, and the *ee* of the crystals recovered in a couple of cycles. This trend, observed in the following cycles as well, suggests the mechanism of enrichment in semi-continuous deracemization.

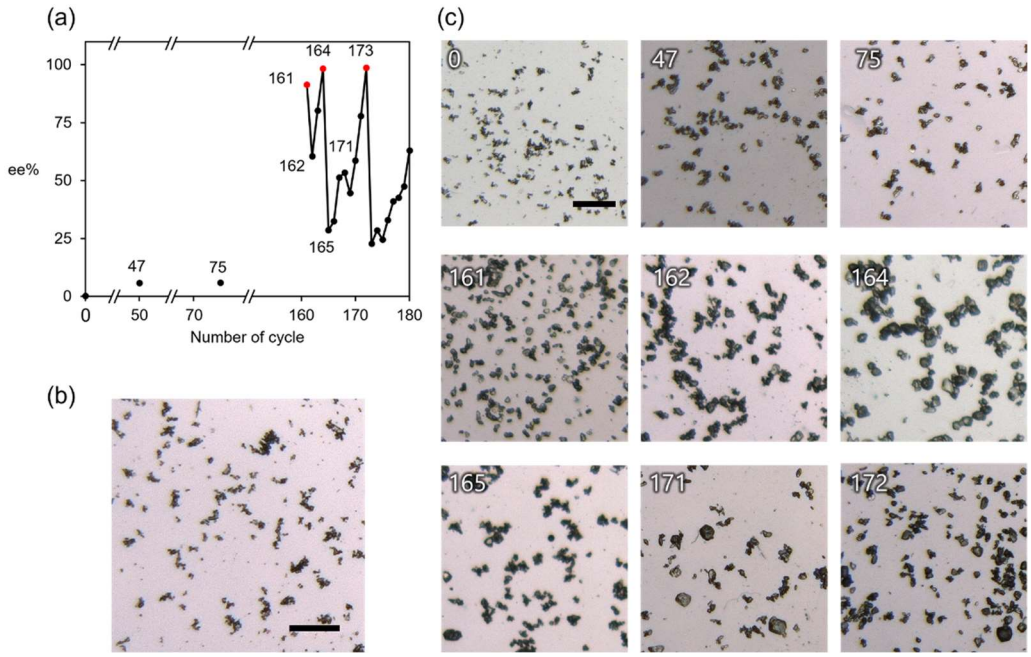

Figure 6. (a) Evolution of *ee* during semi-continuous TCID for the condition of suspension density with 5.3 $\times 10^{-2}$ kg·kg^{-1}. The number on the symbols indicate the number of cycles. (b) Microscopic image of crystals in racemic suspension to be added after enrichment. (c) Microscopic images of crystals during semi-continuous TCID. The numbers on the images corresponds to the number of cycles. Scale bar indicate 100 μm.

To summarize the mechanism of enrichment during the semi-continuous mode could be described by following, as shown in Figure 7. At the beginning of the experiment, tiny racemic crystals exist. Among these,

the smaller crystals dissolve and recrystallize to be incorporated into larger crystals, leading to their gradual growth. Once the crystals reach a certain size, in this system 25–30 μm, fluctuations of the crystal size lead to the predominant growth of crystals with single chirality. This progression gradually achieves the initial enrichment. Subsequently, when a suspension of tiny racemic crystals is added, these tiny crystals aggregate around the already existing larger crystals. Applying temperature cycles causes the tiny crystals to dissolve and be incorporated into nearby crystals, rapidly recovering the *ee*. Namely, the direction of the enrichment is controlled by the chirality of larger crystals. The semi-continuous TCID herein investigated left the enriched crystals of significant size, thanks to this procedure, the chirality of the crystals is controlled to the single enantiomer and the stable continuous production was achieved.

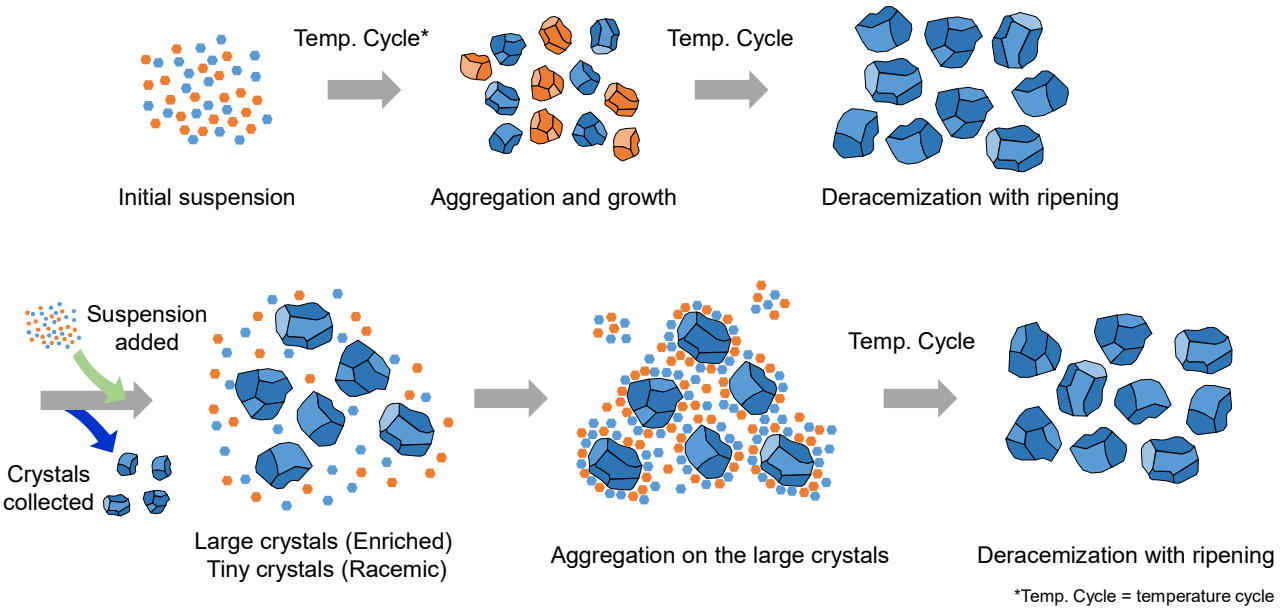

Figure 7. The change of the crystal size and enrichment process behind the semi-continuous deracemization.

Conclusions

In this study, we experimentally validated the semi-continuous operation of deracemization using a batch crystallizer by the simple process of collection and adding suspension. Initially, batch-type TCID was conducted to confirm the correlation between suspension density and productivity during initial enrichment. It was observed in the batch mode TCID that a moderate suspension density yields high productivity, and attention was focused on whether similar behavior would be observed in semi-continuous operation. In the semi-continuous operation experiment, as the scale increased, the initial enrichment took longer period. However, once the *ee* in the crystals enriched, the stable operation could be started. The collection of enriched suspension and addition of racemic suspension can be repeated, achieving successful semi-continuous deracemization. It was also confirmed that the semi-continuous operation provides greater productivity than the batch mode deracemization. Concerning the correlation with suspension density, while the optimal value for the batch mode was different than for the semi-continuous mode, it was provided under moderate conditions. This suggests that the optimal conditions of batch mode TCID offer conditions close to the optimal operating conditions of semi-

continuous TCID, implying its appropriateness for preliminary considerations in efficient scaling up. Furthermore, tracking the crystal particle size revealed the mechanism of enrichment during semi-continous deracemization. The initial enrichment proceeded through the ripening of microcrystals, and after the addition of racemic suspension, numerous microcrystals aggregated on the grown crystals and were incorporated accompanying enrichment. While the exact values are influenced by stirring speed and temperature cycle rate, there is potential for the development of online analysis method to monitor progress of deracemization. These results demonstrate the possibility of converting to continuous crystallization using only simple operations with existing batch crystallizers, which could promote the shift to continuous production in the chemical manufacturing industry.

Associate content

Supporting Information. Solubility data of **1** (PDF).

Author information

Corresponding authors

E-mail: r.oketani.es@osaka-u.ac.jp / i.hisaki.es@osaka-u.ac.jp

ORCID

Ryusei Oketani: 0000-0001-7860-2456
Ichiro Hisaki: 0000-0002-8170-5605

Conflicts of interest

There are no conflicts to declare.

Acknowledgements

This work was supported by KAKENHI (JP 21H01919, JP21K20534, JP23H04593, JP23K13708) from JSPS, a project JPNP20004 by NEDO, and JST ACT-X (JPMJAX22A2). R.O. thanks Multidisciplinary Research Laboratory System for Future Developments (MRL), Graduate School of Engineering Science, Osaka University.

References

(1) Porta, R.; Benaglia, M.; Puglisi, A. Flow Chemistry: Recent Developments in the Synthesis of Pharmaceutical Products. *Org. Process Res. Dev.* **2016**, *20*, 2–25.
(2) Capaldo, L.; Wen, Z.; Noël, T. A Field Guide to Flow Chemistry for Synthetic Organic Chemists. *Chem. Sci.* **2023**, *14*, 4230–4247.
(3) Masui, H.; Fuse, S. Recent Advances in the Solid- and Solution-Phase Synthesis of Peptides and Proteins Using Microflow Technology. *Org. Process Res. Dev.* **2022**, *26*, 1751–1765.

(4) Domokos, A.; Nagy, B.; Szilágyi, B.; Marosi, G.; Nagy, Z. K. Integrated Continuous Pharmaceutical Technologies—A Review. *Org. Process Res. Dev.* **2021**, *25*, 721–739.

(5) Lorenz, H.; Seidel-Morgenstern, A. Processes to Separate Enantiomers. *Angew. Chem. Int. Ed*. **2014**, *53*, 1218–1250.

(6) ter Horst, J. H.; Schmidt, C.; Ulrich, J. 32 - Fundamentals of Industrial Crystallization. In *Handbook of Crystal Growth (Second Edition)*; Rudolph, P., Ed.; Elsevier: Boston, **2015**; pp 1317–1349.

(7) Lawton, S.; Steele, G.; Shering, P.; Zhao, L.; Laird, I.; Ni, X.-W. Continuous Crystallization of Pharmaceuticals Using a Continuous Oscillatory Baffled Crystallizer. *Org. Process Res. Dev.* **2009**, *13*, 1357–1363.

(8) Chen, J.; Sarma, B.; Evans, J. M. B.; Myerson, A. S. Pharmaceutical Crystallization. *Cryst. Growth Des.* **2011**, *11*, 887–895.

(9) Rougeot, C.; Hein, J. E. Application of Continuous Preferential Crystallization to Efficiently Access Enantiopure Chemicals. *Org. Process Res. Dev.* **2015**, *19*, 1809–1819.

(10) Dunn, A. S.; Svoboda, V.; Sefcik, J.; ter Horst, J. H. Resolution Control in a Continuous Preferential Crystallization Process. *Org. Process Res. Dev.* **2019**, *23*, 2031–2041.

(11) G. Coquerel, R. Bouaziz, M. J. Brienne. Optical Resolution of (±)-Fenfluramine and (±)-Norfenfluramine by Preferential Crystallization. *Chem. Lett.* **1988**, *17*, 1081–1084.

(12) Mbodji, A.; Gbabode, G.; Sanselme, M.; Couvrat, N.; Leeman, M.; Dupray, V.; Kellogg, R. M.; Coquerel, G. Family of Conglomerate-Forming Systems Composed of Chlocyphos and Alkyl-Amine. Assessment of Their Resolution Performances by Using Various Modes of Preferential Crystallization. *Cryst. Growth Des.* **2019**, *19*, 5173–5183.

(13) Harfouche, L. C.; Brandel, C.; Cartigny, Y.; Petit, S.; Coquerel, G. Resolution by Preferential Crystallization of Proxyphylline by Using Its Salicylic Acid Monohydrate Co-crystal. *Chem. Eng. Technol.* **2020**, *43*, 1093‑1098.

(14) Zhou, F.; Shemchuk, O.; Charpentier, M. D. Simultaneous Chiral Resolution of Two Racemic Compounds by Preferential Cocrystallization. *Angew. Chem. Int. Ed*. **2021**, *60*, 20264–20268.

(15) Cascella, F.; Temmel, E.; Seidel-Morgenstern, A.; Lorenz, H. Efficient Resolution of Racemic Guaifenesin via Batch-Preferential Crystallization Processes. *Org. Process Res. Dev.* **2020**, *24*, 50–58.

(16) Quon, J. L.; Zhang, H.; Alvarez, A.; Evans, J.; Myerson, A. S.; Trout, B. L. Continuous Crystallization of Aliskiren Hemifumarate. *Cryst. Growth Des.* **2012**, *12*, 3036–3044.

(17) Galan, K.; Eicke, M. J.; Elsner, M. P.; Lorenz, H.; Seidel-Morgenstern, A. Continuous Preferential Crystallization of Chiral Molecules in Single and Coupled Mixed-Suspension Mixed-Product-Removal Crystallizers. *Cryst. Growth Des.* **2015**, *15*, 1808–1818.

(18) Majumder, A.; Nagy, Z. K. A Comparative Study of Coupled Preferential Crystallizers for the Efficient Resolution of Conglomerate-Forming Enantiomers. *Pharmaceutics* **2017**, *9*, 55.

(19) Temmel, E.; Eicke, M. J.; Cascella, F.; Seidel-Morgenstern, A.; Lorenz, H. Resolution of Racemic Guaifenesin Applying a Coupled Preferential Crystallization-Selective Dissolution Process: Rational Process Development. *Cryst. Growth Des.* **2019**, *19*, 3148–3157.

(20) Levilain, G.; Eicke, M. J.; Seidel-Morgenstern, A. Efficient Resolution of Enantiomers by Coupling Preferential Crystallization and Dissolution. Part 1: Experimental Proof of Principle. *Cryst. Growth Des.* **2012**, *12*, 5396–5401.

(21) Temmel, E.; Gänsch, J.; Seidel-Morgenstern, A.; Lorenz, H. Systematic Investigations on Continuous Fluidized Bed Crystallization for Chiral Separation. *Crystals* **2020**, *10*, 394.

(22) Gänsch, J.; Huskova, N.; Kerst, K.; Temmel, E.; Lorenz, H.; Mangold, M.; Janiga, G.; Seidel-Morgenstern, A. Continuous Enantioselective Crystallization of Chiral Compounds in Coupled Fluidized Beds. *Chem. Eng. J.* **2021**, *422*, 129627.

(23) Huskova, N.; Mangold, M.; Seidel-Morgenstern, A. Optimization of a Continuous Fluidized Bed Process for the Separation of Enantiomers by Preferential Crystallization. In *Computer Aided Chemical Engineering*; Türkay, M., Gani, R., Eds.; Elsevier, 2021; Vol. 50, pp 381–386.

(24) Coquerel, G. Preferential Crystallization. *Top. Curr. Chem.* **2007**, *269*, 1–51.

(25) Coquerel, G. Chiral Discrimination in the Solid State: Applications to Resolution and Deracemization. In *Advances in Organic Crystal Chemistry: Comprehensive Reviews 2015*; Tamura, R., Miyata, M., Eds.; Springer Japan: Tokyo, **2015**; pp 393–420.

(26) Viedma, C. Chiral Symmetry Breaking during Crystallization: Complete Chiral Purity Induced by Nonlinear Autocatalysis and Recycling. *Phys. Rev. Lett.* **2005**, *94*, 065504.

(27) Xiouras, C.; Van Aeken, J.; Panis, J.; Ter Horst, J. H.; Van Gerven, T.; Stefanidis, G. D. Attrition-Enhanced Deracemization of NaClO3: Comparison between Ultrasonic and Abrasive Grinding. *Cryst. Growth Des.* **2015**, *15*, 5476–5484.

(28) Oketani, R.; Marin, F.; Tinnemans, P.; Hoquante, M.; Laurent, A.; Brandel, C.; Cardinael, P.; Meekes, H.; Vlieg, E.; Geerts, Y.; Coquerel, G. Deracemization in a Complex Quaternary System with a Second-Order Asymmetric Transformation by Using Phase Diagram Studies. *Chem. Eur. J.* **2019**, *25*, 13890–13898.

(29) Guillot, M.; de Meester, J.; Huynen, S.; Collard, L.; Robeyns, K.; Riant, O.; Leyssens, T. Cocrystallization-Induced Spontaneous Deracemization: A General Thermodynamic Approach to Deracemization. *Angew. Chem. Int. Ed*. **2020**, *59*, 11303–11306.

(30) Valenti, G.; Tinnemans, P.; Baglai, I.; Noorduin, W. L.; Kaptein, B.; Leeman, M.; Ter Horst, J. H.; Kellogg, R. M. Combining Incompatible Processes for Deracemization of a Praziquantel Derivative under Flow Conditions. *Angew. Chem. Int. Ed*. **2021**, *60*, 5279–5282.

(31) Uemura, N.; Yoshida, Y.; Mino, T.; Sakamoto, M. Crystallization-Induced Diastereomer Transformation of Thiohydantoin Derivatives. *Tetrahedron* **2020**, *76*, 131166.

(32) Sanada, K.; Washio, A.; Ishikawa, H.; Yoshida, Y.; Mino, T.; Sakamoto, M. Chiral Symmetry Breaking of Monoacylated Anhydroerythritols and Meso-1,2-Diols through Crystallization-Induced Deracemization. *Angew. Chem. Int. Ed*. **2022**, *61*, e202201268.

(33) Noorduin, W. L.; Izumi, T.; Millemaggi, A.; Leeman, M.; Meekes, H.; Van Enckevort, W. J. P.; Kellogg, R. M.; Kaptein, B.; Vlieg, E.; Blackmond, D. G. Emergence of a Single Solid Chiral State from a Nearly Racemic Amino Acid Derivative. *J. Am. Chem. Soc.* **2008**, *130*, 1158–1159.

(34) Li, W. W.; Spix, L.; de Reus, S. C. A.; Meekes, H.; Kramer, H. J. M.; Vlieg, E.; ter Horst, J. H.

Deracemization of a Racemic Compound via Its Conglomerate-Forming Salt Using Temperature Cycling. *Cryst. Growth Des.* **2016**, *16*, 5563–5570.

(35) Suwannasang, K.; Flood, A. E.; Rougeot, C.; Coquerel, G. Using Programmed Heating–Cooling Cycles with Racemization in Solution for Complete Symmetry Breaking of a Conglomerate Forming System. *Cryst. Growth Des.* **2013**, *13*, 3498–3504.

(36) Cameli, F.; Xiouras, C.; Stefanidis, G. D. Intensified Deracemization via Rapid Microwave-Assisted Temperature Cycling. *CrystEngComm* **2018**, *20*, 2897–2901.

(37) Engwerda, A. H. J.; Maassen, R.; Tinnemans, P.; Meekes, H.; Rutjes, F. P. J. T.; Vlieg, E. Attrition-Enhanced Deracemization of the Antimalaria Drug Mefloquine. *Angew. Chem. Int. Ed*. **2019**, *58*, 1670–1673.

(38) Bodák, B.; Maggioni, G. M.; Mazzotti, M. Effect of Initial Conditions on Solid-State Deracemization via Temperature Cycles: A Model-Based Study. *Cryst. Growth Des.* **2019**, *19*, 6552–6559.

(39) Bodák, B.; Maggioni, G. M.; Mazzotti, M. Population-Based Mathematical Model of Solid-State Deracemization via Temperature Cycles. *Cryst. Growth Des.* **2018**, *18*, 7122–7131.

(40) Bodák, B.; Mazzotti, M. Solid-State Deracemization via Temperature Cycles in Continuous Operation: Model-Based Process Design. *Cryst. Growth Des.* **2022**, *22*, 1846–1856.

(41) Iggland, M.; Mazzotti, M. A Population Balance Model for Chiral Resolution via Viedma Ripening. *Cryst. Growth Des.* **2011**, *11*, 4611–4622.

(42) Katsuno, H.; Uwaha, M. Effect of Nucleation on Chirality Conversion Induced by Random Fluctuation. *J. Cryst. Growth* **2014**, *401*, 59–62.

(43) Uwaha, M. A Model for Complete Chiral Crystallization. *J. Phys. Soc. Jpn.* **2004**, 73, 2601–2603.

(44) Uwaha, M. Simple Models for Chirality Conversion of Crystals and Molecules by Grinding. *J. Phys. Soc. Jpn.* **2008**, *77*, 083802.

(45) Cameli, F.; Xiouras, C.; Stefanidis, G. D. High-Throughput on Demand Access of Single Enantiomers by a Continuous Flow Crystallization Process. *CrystEngComm* **2020**, *22*, 3519–3525.

(46) Bodák, B.; Breveglieri, F.; Mazzotti, M. Crystallization-Induced Deracemization: Experiments and Modeling. *Cryst. Growth Des*. **2022**, *22*, 1427–1436.

(47) Sakamoto, M.; Unosawa, A.; Kobaru, S.; Saito, A.; Mino, T.; Fujita, T. Asymmetric Photocycloaddition in Solution of a Chiral Crystallized Naphthamide. *Angew. Chem. Int. Ed*. **2005**, *44*, 5523–5526.

(48) Kondepudi, D. K.; Asakura, K. Chiral Autocatalysis, Spontaneous Symmetry Breaking, and Stochastic Behavior. *Acc. Chem. Res.* **2001**, *34*, 946–954.

(49) Noorduin, W. L.; Meekes, H.; van Enckevort, W. J. P.; Millemaggi, A.; Leeman, M.; Kaptein, B.; Kellogg, R. M.; Vlieg, E. Complete Deracemization by Attrition-Enhanced Ostwald Ripening Elucidated. *Angew. Chem. Int. Ed*. **2008**, *47*, 6445–6447.